VOLTAGE-FREQUENCY STABILITY ANALYSIS OF A LOW INERTIA ELECTRICAL GRID USING A KURAMOTO-LIKE MODEL

Robert Pollak
University of Ottawa, Canada
Rpoll020@uottawa.ca

Javad Fattahi
University of Ottawa, Canada
Javad.Fattahi@uottawa.ca

Henry Schriemer
University of Ottawa, Canada
hschriemer@uottawa.ca

ABSTRACT

This paper investigates the voltage and phase dynamics of a low inertia inverter based Microgrid in islanded operation. In such case, the network is less robust to disturbances due to the lack of associated inertia within an inverter. In islanded operation the assumption of a stiff grid is no longer valid and the voltage and phase adjustment based on conventional droop control have a resulting effect on the power flows throughout the network where voltage and frequency stability of the network may be compromised. Other approaches neglect the network dynamics when there are power imbalances in the system and how each node is affected and if the resulting increase in demand can be met with the available generation. This paper uses the fact that the phase dynamics of coupled inverters that employ droop control closely resemble the phase dynamics proposed by the Kuramoto model. Using this model allows the network stability to be analysed under the true nonlinear operation. We find through the strong coupling impedance of the primary distribution transmission lines and the implementation of robust droop control provides an appropriate means for rural and suburban neighbourhoods to operate independently.

INTRODUCTION

The electric power system (EPS) was originally designed in consideration of centralized generation with one-way power flows. Renewable energy has become essential to meet increasing energy demands in a clean and sustainable fashion, leading to a high penetration of distributed energy resources (DER) such as photovoltaic (PV) and wind power systems which are interfaced to the grid through inverters. DER penetration is typically done at the distribution level and therefore introduces two-way power flow into the utility grid.

When DERs were first being introduced into the distribution grid it was not anticipated that DERs would have significant impact on local EPS. It was therefore assumed that the frequency and voltage at the substation between the distribution and transmission grid would remain close to nominal no matter how these DERs would contribute. Early standards for inverter technology were based on the "do no harm" principle where the DER should not actively regulate frequency or voltage at the point of common coupling (PCC) and thus would cease to energize the area EPS when voltage and frequency fell out of defined limits. With rapidly increasing amounts of DER in the utility grid, these strict operating requirements are eliminating the added benefits of increased DER penetration and may present negative effects on the bulk power system (BPS). Where BPS concerns are frequency regulation, utility/local level concerns are voltage regulation. The latest revision of interconnection standards, such as [1], now mandate DER flexibility in which these systems must meet certain voltage and frequency ride through requirements. The newest revision also mandates reactive power injection capability allowing DERs to regulate voltage at the PCC.

In islanded operation when a Microgrid is formed, frequency regulation becomes an added concern for the local utility/distributed resources. Due to the non-inertial based generation sources, the microgrid becomes very sensitive to load/generation changes and abnormal events, creating serious reliability issues within the EPS. System frequency is similar across the entire interconnection and is established by the balance between load and generation. So, any loss in DER will have an impact on the system frequency, requiring other resources to address the deviation. Furthermore, these events may cause voltage reduction on buses and challenge the capability of each DER unit to meet the demands at the PCC.

Modelling and analysis performed in [4] provides a complete small signal microgrid model and stability analysis, where the model was linearized around an operating point. Their model was simulated and verified for multiple parallel connected electronic based generation sources in which the electronic generators were determined to be sensitive to network configuration and dynamics, load dynamics, inner control loops and droop coefficients depending on the parameter settings of each electronic generator. Their results demonstrate the operational capability of distributed generation to sustain local demand under small signal stability. The inherent model limitations specifically restrict the stability analysis to small disturbances in which a linear model approximation is still valid. We address network operation under large signal conditions.

Previous work [2] provides a frequency stability and synchronization analysis regarding the operation of an inertia-based multi-machine power grid in which a relationship was formed between the phase dynamics of a multi-machine system and a Kuramoto-like model. In modern distribution systems, low-inertia based generation dominates the distribution network generation capacity. An operational analysis [3] into a microgrid scenario consisting of rotating machines and power electronic

based generation provides an stability analysis. Furthermore, their analysis demonstrated the effect of different line impedance amongst the single feeder interconnection of separated microgrids, and their conclusion implied that certain cables caused the system to become unstable for some significant load steps. In residential areas where rooftop PV installation capacity is increasing rapidly, the low voltage networks consist primarily of low inertia based generation in which power flows from the generation into the network are based on the characteristics of a resistive dominated line.

This paper expands on the works performed in [2,3]. We perform a microgrid stability analysis on a neighbourhood with only power electronics based PV generation sources. Furthermore, a piece-wise linear volt-watt droop curve is proposed to increase the robustness of the system. This allows the generation sources to more easily maintain system integrity despite power flow being load dominated. These sources are interconnected throughout the distribution network via a ring connection. Each home has specific PV generation capacity and loads that are aggregated at the PCC (*i.e.*, the distribution panel). If the generation capacity is not sufficient to self-sustain its local loads , it must import/export power through the network in order to balance demands.

The interconnection between homes are through medium voltage lines (*i.e.*, primary distribution transmission lines) which establish the neighbourhood power flow. The rooftop PV systems are connected at the low-voltage level where power flows to the POC are governed by the impedance of a LV line. Several disturbance tests are performed throughout the network in which generation, loading and interconnection are adjusted to analyse the transient large signal network stability.

NETWORK MODEL

Droop Controlled Inverter Model

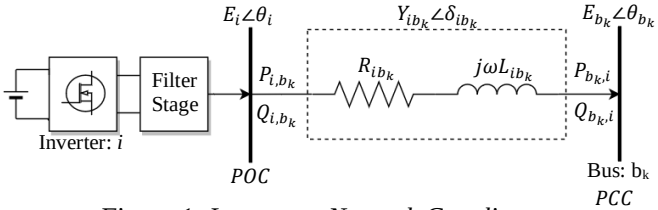

Figure 1: Inverter to Network Coupling

In a microgrid scenario, inverters are typically connected at the secondary distribution voltage level where the transmission of active and reactive power between two oscillators i, k are governed by the line impedance as

$$\left|Y_{i_ib_k}\right|e^{j\delta_{i_ib_k}} = Y_{i_ib_k}\cos(\delta_{i_ib_k}) + jY_{i_ib_k}\sin(\delta_{i_ib_k}) \quad (1)$$

$$= G_{i_ib_k} + jB_{i_ib_k},$$

where $Y_{i_ib_k}$, $G_{i_ib_k}$ and $B_{i_ib_k}$ are the line admittance, conductance and susceptance, respectively, between inverter i_i and network bus b_k, which may both be characterized as oscillators. For notational clarity, $(\cdot)_{i_ib_k}$ denotes the coupling between the i_{th} inverter and the b_{kth} network bus and furthermore, $(\cdot)_{i_i,b_k}$ is a directional representation from the i_{th} inverter to the b_{kth} bus and vice versa.

Modern inverters that employ droop control have their corresponding droop curves configured by the properties of the coupling admittance, $\left|Y_{i_ib_k}\right|e^{j\delta_{i_ib_k}}$, of the inverter to the PCC itself. If the voltage at the grid edge is low, the line impedance is typically dominated by the resistive component of the line [6,7]. Droop controlled inverters employ their corresponding settings based on this property, and the power flow between the two oscillators may then be characterized as

$$P_{i_i,b_k} = G_{i_ib_k}E_{i_i}(E_{i_i} - E_{b_k}\cos(\theta_{i_i} - \theta_{b_k})) \quad (2)$$

$$Q_{i_i,b_k} = -G_{i_ib_k}E_{i_i}E_{b_k}\sin(\theta_{i_i} - \theta_{b_k}), \quad (3)$$

where P_{i_i,b_k} and Q_{i_i,b_k} denote the active and reactive power injection, respectively (*i.e.*, the transmitted power from the i_{th} inverter to the b_{kth} bus). NB, (2) and (3) only characterize the power flows between two oscillators but do not characterize the power flows throughout a network. Equations (2) and (3) demonstrate two things: first, that the active power injected from the i_{th} inverter into to a stiff network bus strongly depends on the difference between voltage amplitudes of the two oscillators; and second, that the reactive power injection depends strongly on the difference between their respective voltage phase angles. Due to these properties, the droop curves employed by each inverter may be configured as

$$E_{i_i} = -m_{i_i}(P_{i_i,b_k} - P_{i_i,nom}) + {E_{i_i}}^* \quad (4)$$

$$\omega_{i_i} = n_{i_i}(Q_{i_i,b_k}) + {\omega_{i_i}}^* \quad , \quad (5)$$

where ${E_{i_i}}^*$ is the inverter operating voltage set point for nominal power injections of $P_{i_i,nom}$ (this nominal power set point is determined by both the generation capacity and the network operator responsible for governing the interconnection requirements); ${\omega_{i_i}}^*$ is the nominal operating frequency set point; E_{i_i} and ω_{i_i} are the output voltage and frequency control signal for the inverter based on their respective droop gains m_{i_i} and n_{i_i}; and P_{i_i,b_k} and Q_{i_i,b_k} are the sensed active and reactive output powers, respectively. Furthermore, (4) and (5) may be written as

$$\Delta E_{i_i} = {E_{i_i}}^* - E_{i_i} = m_{i_i}(P_{i_i,b_k} - P_{i_i,nom}) \quad (6)$$

$$\Delta\omega_{i_i} = \omega_{i_i} - {\omega_{i_i}}^* = n_{i_i}Q_{i_i,b_k} \quad . \quad (7)$$

This allows the following intuition to be developed:

The dynamics of a droop-controlled inverter are strictly governed by the droop coefficients and the power flows from the inverter into the network. Any deviation of voltage and frequency from their nominal set point is the result of a power imbalance in the network. For a low voltage microgrid operation in Volt-Watt (V-W) mode (V-W), we propose a piece-wise linear curve where the rate of power curtailment can be made greater for over-voltage conditions than is the case in conventional droop control (where the generator is sensitive to the constant slope droop coefficient). In microgrid operation, any load steps will have a large impact on the system stability so the ability for the generators to stay online is crucial.

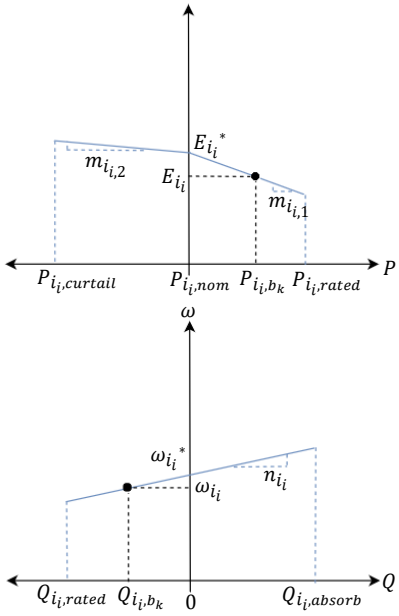

Figure 2: Employed Droop Curves

Inverter Voltage Dynamics

When operating in islanded mode, the stiff grid assumption is no longer valid, therefore the conventional droop control methodology has significant effects on the voltage profile throughout the network. The voltage drops in the network as the load increases and hence the generation voltage may also drop due to the conventional droop control. In order to ensure that the voltage is limited to the required operational range, the voltage error must be feedback into the system by measuring the calculated difference between the inverter reference set point voltage and bus voltage [8,9]. This error is then added as a positive feedback to the existing voltage feedback signal (6) as,

$$\Delta E_{i_i} = K_{E,e}(E_{i_i}{}^* - E_{b_k}) - m_{i_i}(P_{i_i,b_k} - P_{i,nom}) \,. \quad (8)$$

The integration of (8) provides the control signal to the inverter and may be expressed as

$$\tau_{i_i} \frac{dE_{i_i}}{dt} = K_{E,e}(E_{i_i}{}^* - E_{b_k}) - m_{i_i}(P_{i_i,b_k} - P_{i,nom}), \quad (9)$$

where $K_{E,e}$ is the reference voltage error feedback gain and τ_{i_i} captures the delay in the system for the i_{th} inverter [10].

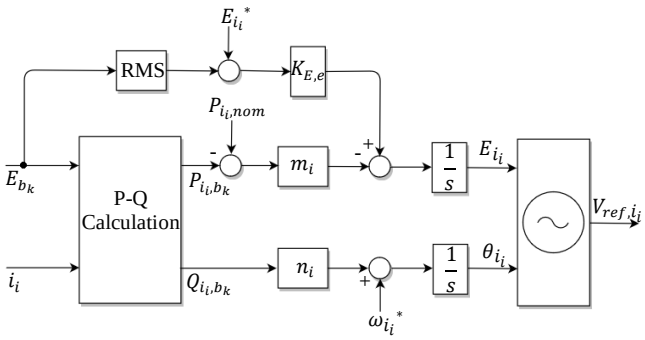

Figure 3: Microgrid Droop Control Schema

The Kuramoto Model

The Kuramoto model was developed to model the phenomenon of collective synchronization of individual oscillators with uniformly distributed natural frequencies around a similar limit cycle. For any system of weakly coupled oscillators, the long-term dynamics are governed by [12]

$$\frac{d\theta_i}{dt} = \omega_i + \sum_{k=1}^{N} \alpha_{ij}(\theta_i - \theta_j) \,. \quad (10)$$

Systems with purely sinusoidal coupling can be represented by

$$\frac{d\theta_i}{dt} = \omega_i + \sum_{k=1}^{N} \kappa_{ij} \sin(\theta_i - \theta_j) \,, \quad (11)$$

where θ_i is phase angle of oscillator i with respect to a stationary reference frame, ω_i is the natural frequency of the oscillator, $\kappa_{ij} \geq 0$ is the coupling gain between oscillators i and j, and $\sin(\theta_i - \theta_j)$ is the phase interaction function. The system is incoherent until coupling gain $\kappa_{ij} > \kappa_{critical}$ whence the system then becomes synchronous. The significance of this model will now be described with respect to a microgrid network.

Microgrid Network Dynamics

Similar to power flows from the inverter into the bus, as presented in the preceding subsections, the power flows within a microgrid network also depend on the voltage amplitudes and phases on their respective buses. The apparent power required from each bus within the network can be expressed as

$$S_{b_k,i_i} = \sum_{k=1}^{N} E_{b_k} E_{b_j} Y_{b_{kj}} e^{j(\theta_{b_k} - \theta_{b_j} - \delta_{b_{kj}})} \,, \quad (12)$$

where the phasors $E_{b_k} e^{j\theta_{b_k}}$ and $E_{b_j} e^{j\theta_{b_j}}$ are the voltage magnitude and angle, respectively, at bus k and j; and $Y_{b_{kj}} e^{j\delta_{b_{kj}}}$ is the admittance of the transmission line between bus k and j. Applying a change of variable $\kappa_{kj} =$

$E_{b_k}E_{b_j}Y_{b_{kj}}$, allows (12) to be written as

$$S_{b_k,i_i} = {E_{b_k}}^2 Y_{b_{kk}} e^{-j\delta_{b_{kk}}} - \sum_{\substack{k=1 \\ k\neq j}}^{N} \kappa_{kj} e^{j\left(\theta_{b_k}-\theta_{b_j}-\delta_{b_{kj}}\right)} \quad (13)$$

where the apparent power injection depends on the driving-point admittance of bus k, denoted by $Y_{b_{kk}} e^{-j\delta_{b_{kk}}}$, and the transfer admittances= between buses i and k, denoted by $Y_{b_{kj}} e^{j\left(\theta_{b_k}-\theta_{b_j}-\delta_{b_{kj}}\right)}$ [11]. These may be conceptualized as follows: the driving-point admittance are the loads directly connected to bus k which may be considered as the local loads and the transfer admittances may be conceptualized as the power flows exported/imported from branch k to j within the network. Furthermore, the power injection at bus k can be demonstrated in terms of active and reactive power as

$$P_{b_k,i_i} = \sum_{k=1}^{N} \kappa_{kj} \cos(\theta_{b_k} - \theta_{b_j} - \delta_{b_{kj}}) \quad (14)$$

$$Q_{b_k,i_i} = -\sum_{k=1}^{N} \kappa_{kj} \sin\left(\theta_{b_k} - \theta_{b_j} - \delta_{b_{kj}}\right). \quad (15)$$

As the phase dynamics of a low voltage network are correlated with the reactive power, the phase dynamics of a converter under resistive dominated coupling may be described by (15) in (7) as

$$\frac{d\theta_{i_i}}{dt} = {\omega_{i_i}}^* - n_i \sum_{k=1}^{N} \kappa_{kj} \sin\left(\theta_{b_k} - \theta_{b_j} - \delta_{b_{kj}}\right), \quad (16)$$

and the voltage dynamics by (14) in (9) as

$$\tau_{i_i} \frac{dE_{i_i}}{dt} = K_{E,e}({E_{i_i}}^* - E_{b_k}) + m_i[P_{i,nom} - \sum_{k=1}^{N} \kappa_{kj} \cos\left(\theta_{b_k} - \theta_{b_j} - \delta_{b_{kj}}\right)] \quad (17)$$

Equation (16) demonstrates that reactive power flows under the resistive coupling impedance assumption very much resemble the Kuramoto model, as shown in (11). Further insight into the Kuramoto model can be developed by writing (16) as

$$\frac{d\theta_i}{dt} = \omega_{n,i} - n_i \sum_{\substack{k=1 \\ k\neq j}}^{N} \kappa_{kj} \sin\left(\theta_{b_k} - \theta_{b_j} - \delta_{b_{kj}}\right), \quad (17)$$

where the natural frequency $\omega_n = {\omega_i}^* - n_i({E_{b_k}}^2 Y_{b_{kk}} \sin(\delta_{b_{kk}}))$ of each inverter (oscillator) depends on the ability for the DER to meet the local demand. This natural frequency is further influenced by the demand/supply required from the network itself which is determined by the network coupling $\kappa_{kj} \sin\left(\theta_{b_k} - \theta_{b_j} - \delta_{b_{kj}}\right)$, where the coupling strength $\kappa_{kj} = E_{b_k}E_{b_j}Y_{b_{kj}}$ between oscillators is characterized by the bus's voltage and coupling impedance magnitudes. The sinusoidal phase interaction between inverters is further influenced by the drift of the line which will always introduce a phase error constant of $\delta_{b_{kj}}$.

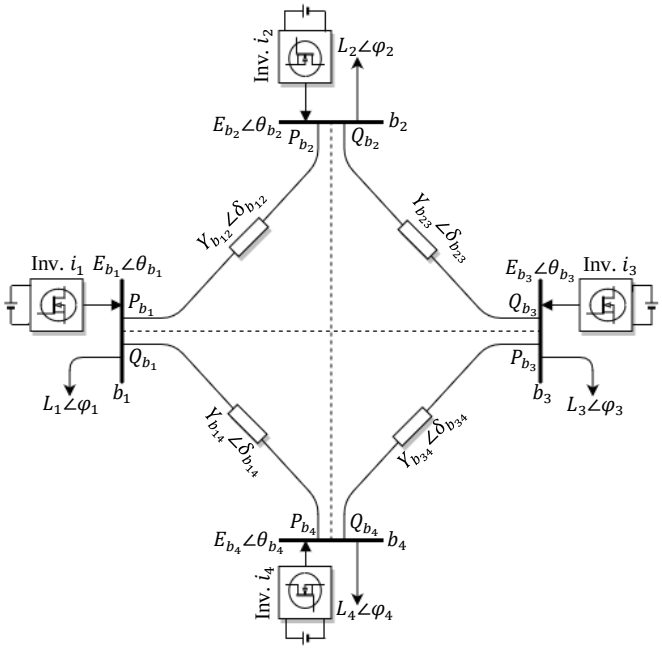

Figure 4: Ring Network Model

CASE STUDIES & RESULTS

The case studies performed in this section are concerned with only large signal stability of the proposed distribution network, shown in Figure 4, in islanded operation. The rated generation capacity on the distribution network is selected to be the average PV rooftop capacity in North America.

Bus (b_k)	Network Settings	
	Rated Active Power ***(P_{b_k,i_i})***	***Rated Reactive Power*** ***(Q_{b_k,i_i})***
b_1	5.0kW	2.2kVAR
b_2	3.0kW	1.32kVAR
b_3	6.0kW	2.64kVAR
b_4	10kW	4.4kVAR
Total:	24kW	10.56kVAR

Table 1: Network Generation Capacity

Short length primary distribution transmission lines have high admittances. Due to the size of the network, the load admittances are relatively small in comparison. Therefore the coupling, κ_{kj}, in the network is dominated by the transmission line. During a forced islanded situation, the phases of the generators in the network are operating at their respective grid connected operating point. When forced into islanded operation, the strong coupling in the network forces the phases to lock almost instantaneously, demonstrated in Figure 5. The steady-state phase error of the buses within the network are based on the reactive power generation/demand at the respective buses, which is small due to this coupling property.

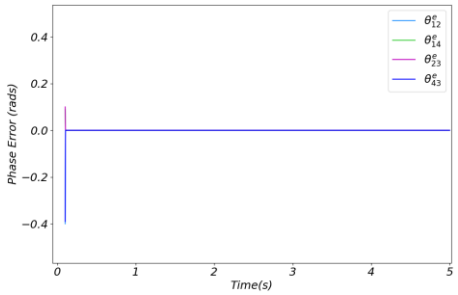

Figure 5: Forced Islanded Operation Phase Error

The results obtained in Figure 5 demonstrate the phase error during a forced islanding operation at $t = 0$, where each generator is operating at 80% of their respective active power. The reactive loading in the network at the network buses are 4.4kVAR at b_1, 1.32kVAR at b_2, 2.64kVAR at b_3 and 2.2kVAR at b_4.

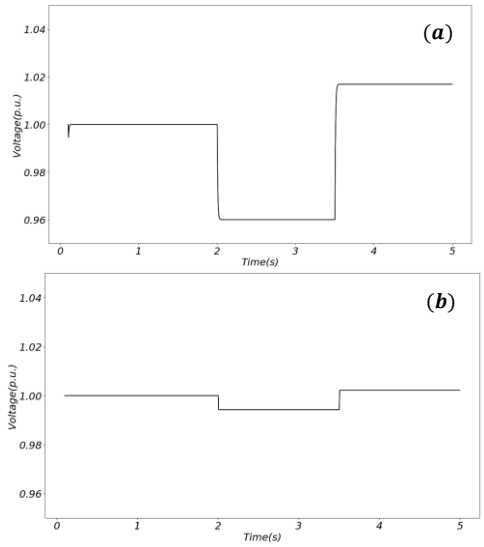

Figure 6: Network Voltage Profile (a) Conventional Droop Control (b) Robust Droop Control

The results obtained in Figure 6 demonstrate the bus voltages throughout the network. During forced islanded operation each generator is operating at rated reactive power and 80% of their respective active power. An active power load step is applied to the network of 3.0kW at b_1, 0.6kW at b_2, 3.2 kW at b_3 and shed of 2.0kW at b_4, for 2 < t < 3.5s. For t > 3.5s there is a significant loss in load where the loading at the buses become, 4.0kW at b_1, 3.0kW at b_2, 2.0kW at b_3 and 8.0kW at b_4. The results for the standard droop controller are shown in Figure 6a, while those for the robust droop controller are shown in Figure 6b, indicating the significant improvement in voltage performance and load sharing.

REFERENCES

[1] *IEEE Standard for Interconnection and Interoperability of Distributed Energy Resources with Associated Electric Power Systems Interfaces*, IEEE Std 1547, 2018

[2] G. Filatrella, A.H. Nielsen, N.F. Pedersen, 2008, "Analysis of a power grid using a Kuramoto-like model", *The European Physical Journal B*, 61, 485-491

[3] Z. Wang, M. Lemmon, 2015, "Stability analysis of weak rural electrification microgrids with droop-controlled rotational and electronic distributed generators", *2015 IEEE Power & Energy Society General Meeting*, IEEE Press, pp. 1-5.

[4] N. Pogaku, M. Prodanovic, T.C. Green, 2007, "Modelling, Analysis and Testing of Autonomous Operation of an Inverter-Based Microgrid", *IEEE Transactions on Power Electronics*, vol.22, No.2

[5] D. Georgakis, S. Papathanassiou, N. Hatziargyiou, A. Engler, Ch. Hardt, 2004, "Operation of a prototype Microgrid system based on micro-sources equipped with fast-acting power electronics interfaces", *Proceedings of IEEE PECS'04*, vol.4, pp. 2521-2526

[6] A. Engler, N. Soultanis 2005, "Droop control in LV-grids", *Proceedings of Future Power Systems, International Conference on*, vol., no., pp. 1-6

[7] J. Rocabert, A. Luna, F. Blaabjerg, P. Rodriguez, 2012, "Control of Power Converters in AC Microgrids", *IEEE Transactions on Power Electronics*, vol.27, no.11, pp. 4734-4748

[8] Q.C. Zhong, T. Hornik, 2013, *Control of Power Inverters in Renewable Energy and Smart Grid Integration*, John Wiley & Sons, West Sussex, United Kingdom, 297-346

[9] Q.C. Zhong, 2013, "Robust Droop Controller for Accurate Propotional Load Sharing Among Inverters Operated in Parallel", *IEEE Transactions on Industrial Electronics*, vol. 60, no 4., pp. 1281-1290

[10] E. Antonio, A. Coelho, P.C. Cortizo, P.F.D. Garcia, 2002, "Small-Signal Stability for Parallel-Connected Inverters in Stand-Alone AC Supply Systems" *IEEE Transactions on Industry Applications*, vol. 38, no. 2, pp. 533-542

[11] J. Machowski, J W. Bialek, J R. Bumby, 2008, *Power System Dynamics – Stability and Control*, 2nd ed., Wiley & Sons, pp20 - 230

[12] S. H. Strogatz, 2000, "From Kuramoto to Crawford: Exploring the onset of Synchronization in Populations of Coupled Oscillators" *Physica D 143*